metals

MDPI

Article

Microstructure, Mechanical Property, and Phase Transformation of Quaternary NiTiFeNb and NiTiFeTa Shape Memory Alloys

Yulong Liang [1,2], Shuyong Jiang [1,*], Yanqiu Zhang [1] and Junbo Yu [2]

[1] College of Mechanical and Electrical Engineering, Harbin Engineering University, Harbin 150001, China; yulongliang380@126.com (Y.L.); zhangyq@hrbeu.edu.cn (Y.Z.)

[2] College of Materials Science and Chemical Engineering, Harbin Engineering University, Harbin 150001, China; yujunbo@hrbeu.edu.cn

* Correspondence: jiangshuyong@hrbeu.edu.cn; Tel.: +86-451-8251-9710

Received: 3 July 2017; Accepted: 9 August 2017; Published: 12 August 2017

Abstract: Based on ternary $Ni_{45}Ti_{51.8}Fe_{3.2}$ (at %) shape memory alloy (SMA), Nb and Ta elements are added to an NiTiFe SMA by replacing Ni element, and consequently quaternary $Ni_{44}Ti_{51.8}Fe_{3.2}Nb_1$ and $Ni_{44}Ti_{51.8}Fe_{3.2}Ta_1$ (at %) SMAs are fabricated. The microstructure, mechanical property, and phase transformation of NiTiFeNb and NiTiFeTa SMAs are further investigated. Ti_2Ni and β-Nb phases can be observed in NiTiFeNb SMA, whereas Ti_2Ni and Ni_3Ti phases can be captured in NiTiFeTa SMA. As compared to NiTiFe SMA, quaternary NiTiFeNb and NiTiFeTa SMAs possess the higher strength, since solution strengthening plays a considerable role. NiTiFeNb and NiTiFeTa SMAs exhibit a one-step transformation from B2 austenite to B19′ martensite during cooling, but they experience a two-step transformation of B19′-R-B2 during heating.

Keywords: shape memory alloy; mechanical property; microstructures; phase transformation

1. Introduction

NiTi shape memory alloys (SMAs) have deserved increasing attention in the domain of engineering since they possess shape memory effect and superelasticity. In general, phase transformation temperature and mechanical property are the two critical factors influencing the application of NiTi SMA in engineering [1–3]. In particular, a third element can be added to the binary NiTi SMA so as to change its phase transformation temperature and mechanical property [4,5]. As a consequence, typical ternary NiTi-based SMAs, such as NiTiCu, NiTiNb, and NiTiFe, have gone toward the engineering application. For instance, NiTiCu SMA possesses a narrow transformation temperature hysteresis, so it can be used in actuators [6–8]. However, NiTiNb SMA possesses a broad transformation temperature hysteresis, so it is suitable for pipe coupling [9–11]. NiTiFe SMA is typically used for coupling pipe since it possesses a lower martensite transformation start temperature [12–14]. NiTiPt, NiTiPd, NiTiZr, and NiTiHf SMAs become candidates for high temperature SMAs since they possess a higher reverse transformation temperature [15–18]. So far, quaternary NiTi-based SMAs have deserved more attention. Some quaternary SMAs have also become potential candidates for high temperature SMAs, such as TiNiPdCu [19], NiTiHfCu [20], NiTiHfZr [21], and NiTiHfTa [22] SMAs. In addition, some new quaternary NiTi-based SMAs, which possess special properties, have been put forward as well. These new quaternary NiTi-based SMAs include NiTiHfPd SMA with high strength [23,24], TiNiCuPd SMA with near-zero hysteresis [25], and NiTiCuV SMA with high thermal stabilization [26]. However, only a few studies have reported the investigations of quaternary NiTi-based SMAs.

In the present study, Nb and Ta elements were added to NiTiFe SMA in order to prepare NiTiFeNb and NiTiFeTa SMAs. Furthermore, the microstructure, mechanical property, and phase transformation of NiTiFeNb and NiTiFeTa SMAs were investigated.

2. Materials and Methods

On the basis of ternary $Ni_{45}Ti_{51.8}Fe_{3.2}$ (at %) SMA, Nb and Ta elements were added by replacing the Ni element, and consequently quaternary $Ni_{44}Ti_{51.8}Fe_{3.2}Nb_1$ and $Ni_{44}Ti_{51.8}Fe_{3.2}Ta_1$ (at %) SMAs were fabricated via the vacuum arc melting method. Then, three as-cast NiTi-based SMAs were heated to 1000 °C and maintained for 12 h. Subsequently, the three heat-treated NiTi-based SMA samples were quenched with ice water. NiTi-based SMA samples, whose height and diameter were 6 mm and 4 mm, respectively, were removed from the heat-treated NiTi-based SMA ingots using electro-discharge machining (EDM) for the purpose of compression tests. The compression tests were performed with INSTRON-5500R equipment (Instron Corporation, Norwood, MA, USA) at room temperature, where the compression strain rate was determined as 0.001 s^{-1}.

Differential scanning calorimetry (DSC) was used to determine the phase transformation temperatures of the three heat-treated NiTi-based SMA specimens by using a Pyris Diamond type differential scanning calorimeter (Perkin Elmer Inc., Waltham, MA, USA). Therein, DSC measurement temperature ranged from −150 °C to 150 °C, and the heating and cooling rates were determined as 10 °C/min.

Optical microscopy (OM) as well as transmission electron microscopy (TEM) was employed to characterize the microstructures of the three heat-treated NiTi-based SMA samples. The samples for the OM experiment were etched in a solution whose composition was determined as $HF:HNO_3:H_2O$ = 1:2:10. Then, the OM experiment was performed using an OLYMPUS311 type optical microscope (Olympus Corporation Tokyo, Japan). The TEM experiment was carried out on an FEI TECNAI G2 F30 microscope (FEI Corporation, Hillsboro, OR, USA) with a side-entry and double-tilt specimen stage with an angular range of ± 40° at an accelerating voltage of 300 kV. Foils for TEM observation were mechanically ground to 70 μm and then thinned by twin-jet polishing in an electrolyte containing 90% C_2H_5OH and 10% $HClO_4$ by volume fraction.

Employing a Philips X'Pert Pro diffractometer (Royal Dutch Philips Electronics Ltd. Amsterdam, Netherlands) with CuKα radiation at ambient temperature, X-ray diffraction (XRD) analysis was used to identify the phase composition of the three heat-treated NiTi-based SMA samples. The samples were scanned over 2θ, which ranges from 20° to 90° by continuous scanning based on a tube voltage of 40 kV and a tube current of 40 mA.

3. Results and Discussion

3.1. Microstructure Analysis of NiTi-based SMAs

Figure 1 shows the microstructures of $Ni_{45}Ti_{51.8}Fe_{3.2}$, $Ni_{44}Ti_{51.8}Fe_{3.2}Nb_1$, and $Ni_{44}Ti_{51.8}Fe_{3.2}Ta_1$ SMAs determined by OM. The microstructures of the three NiTi-based SMAs are dominated by equiaxed grains rather than dendrites. In addition, there are some precipitates in the grain interior as well as at the grain boundary.

To further determine the phase composition of the three NiTi-based SMAs, XRD maps of $Ni_{45}Ti_{51.8}Fe_{3.2}$, $Ni_{44}Ti_{51.8}Fe_{3.2}Nb_1$, and $Ni_{44}Ti_{51.8}Fe_{3.2}Ta_1$ SMAs are illustrated in Figure 2. It is evident that the three NiTi-based SMAs are composed of B2 austenite and Ti_2Ni precipitate.

In order to gain an in-depth insight into the microstructures of the three NiTi-based SMAs, TEM micrographs of $Ni_{45}Ti_{51.8}Fe_{3.2}$, $Ni_{44}Ti_{51.8}Fe_{3.2}Nb_1$, and $Ni_{44}Ti_{51.8}Fe_{3.2}Ta_1$ SMAs are shown in Figures 3–5, respectively. It can be observed from Figure 3 that $Ni_{45}Ti_{51.8}Fe_{3.2}$ SMA consists of B2 austenite matrix and Ti_2Ni precipitate. It can be seen in Figure 4 that in terms of $Ni_{44}Ti_{51.8}Fe_{3.2}Nb_1$ SMA, Ti_2Ni and β-Nb precipitates occur in the matrix of B2 austenite. It can be seen in Figure 5 that the matrix of $Ni_{44}Ti_{51.8}Fe_{3.2}Ta_1$ SMA belongs to B2 austenite, where both Ti_2Ni and Ni_3Ti precipitates can be observed.

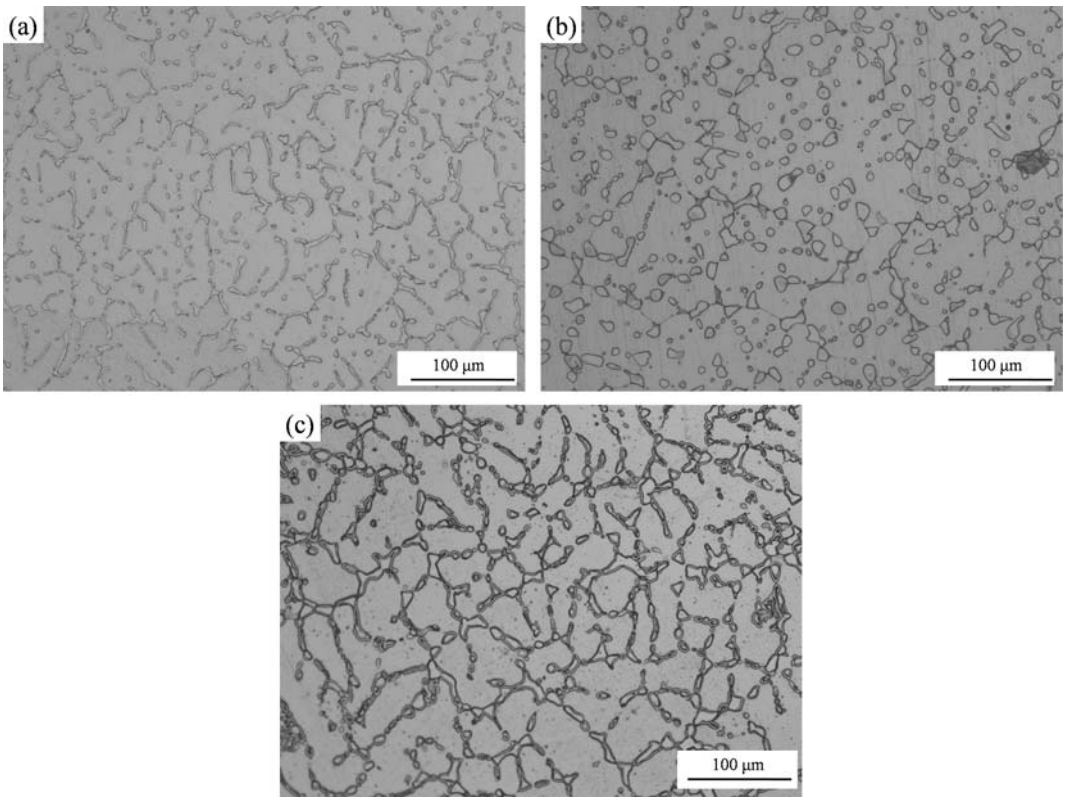

Figure 1. OM (Optical microscopy) micrographs of the three NiTi-based SMAs: (**a**) $Ni_{45}Ti_{51.8}Fe_{3.2}$; (**b**) $Ni_{44}Ti_{51.8}Fe_{3.2}Nb_1$; (**c**) $Ni_{44}Ti_{51.8}Fe_{3.2}Ta_1$.

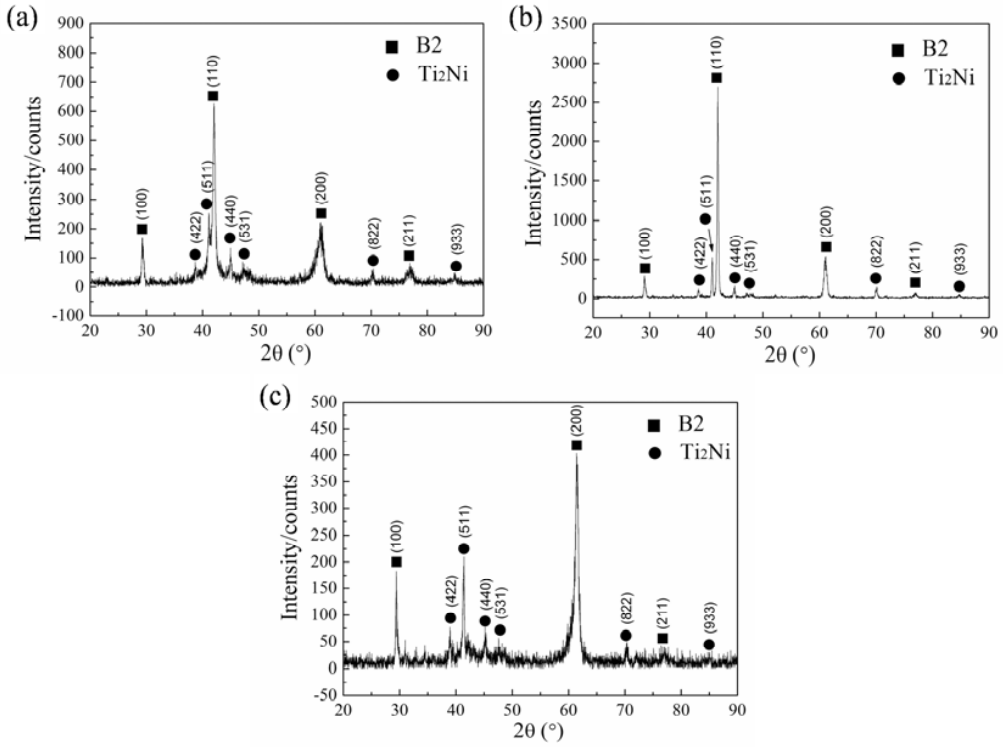

Figure 2. XRD (X-ray diffraction) maps of the three NiTi-based SMAs: (**a**) $Ni_{45}Ti_{51.8}Fe_{3.2}$; (**b**) $Ni_{44}Ti_{51.8}Fe_{3.2}Nb_1$; (**c**) $Ni_{44}Ti_{51.8}Fe_{3.2}Ta_1$.

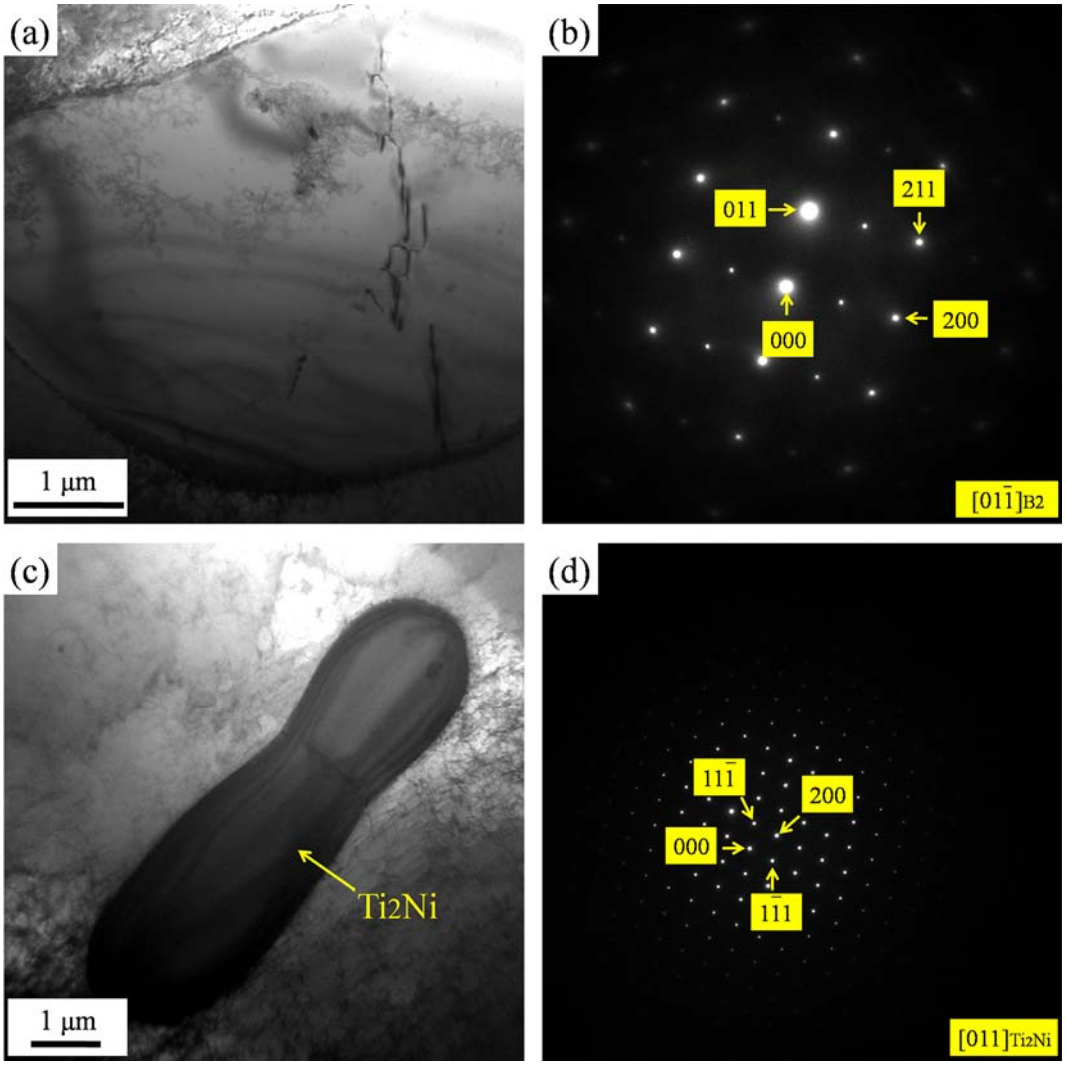

Figure 3. TEM (Transmission electron microscopy) micrographs of $Ni_{45}Ti_{51.8}Fe_{3.2}$ SMA (Shape memory alloy): (**a**) Bright field image showing B2 austenite matrix; (**b**) Diffraction pattern of B2 austenite matrix in (**a**); (**c**) Bright field image showing Ti_2Ni precipitate; (**d**) Diffraction pattern of Ti_2Ni precipitate in (**c**).

3.2. Mechanical Property of NiTi-based SMAs

Figure 6 illustrates the stress-strain curves of $Ni_{45}Ti_{51.8}Fe_{3.2}$, $Ni_{44}Ti_{51.8}Fe_{3.2}Nb_1$, and $Ni_{44}Ti_{51.8}Fe_{3.2}Ta_1$ SMAs under uniaxial compression. It is observed that the addition of Nb and Ta elements results in the increasing yield strength of NiTi-based SMAs, but also leads to the decreasing plasticity of NiTi-based SMAs. Furthermore, $Ni_{44}Ti_{51.8}Fe_{3.2}Nb_1$ SMA possesses a higher yield strength than $Ni_{44}Ti_{51.8}Fe_{3.2}Ta_1$ SMA. In other words, the Nb element plays a more substantial role in strengthening NiTi-based SMAs compared with the Ta element. According to the aforementioned microstructural analysis, no metallic compounds of Nb and Ta elements are observed in the case of $Ni_{44}Ti_{51.8}Fe_{3.2}Nb_1$ and $Ni_{44}Ti_{51.8}Fe_{3.2}Ta_1$ SMAs. Consequently, it can be concluded that Nb and Ta exist in the solid solution of B2 austenite as the solute atoms. In particular, compared to $Ni_{45}Ti_{51.8}Fe_{3.2}$ and $Ni_{44}Ti_{51.8}Fe_{3.2}Nb_1$ SMAs, $Ni_{44}Ti_{51.8}Fe_{3.2}Ta_1$ SMA exhibits a steady strain hardening ability during plastic deformation. It is well known that the strain hardening ability of metal materials is related closely to the dislocation density. In general, the strain hardening ability increases with increasing dislocation denstiy. Therefore, as for $Ni_{44}Ti_{51.8}Fe_{3.2}Ta_1$ SMA, plenty of dislocations need to be enhanced so as to guarantee the compatiblity of plastic deformation.

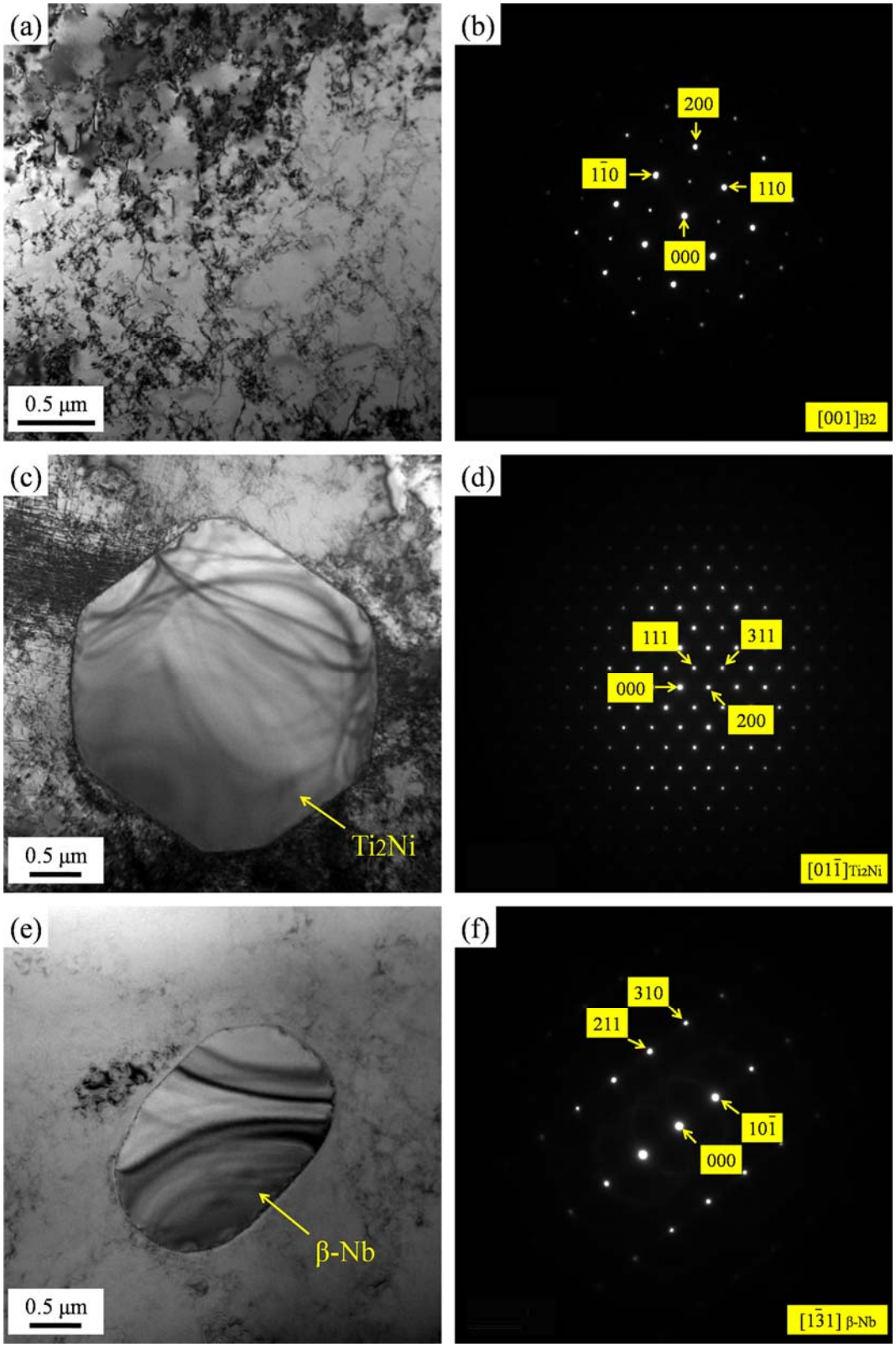

Figure 4. TEM micrographs of $Ni_{44}Ti_{51.8}Fe_{3.2}Nb_1$ SMA: (**a**) Bright field image showing B2 austenite matrix; (**b**) Diffraction pattern of B2 austenite matrix in (**a**); (**c**) Bright field image showing Ti_2Ni precipitate; (**d**) Diffraction pattern of Ti_2Ni precipitate in (**c**); (**e**) Bright field image showing β-Nb precipitate; (**f**) Diffraction pattern of β-Nb precipitate in (**e**).

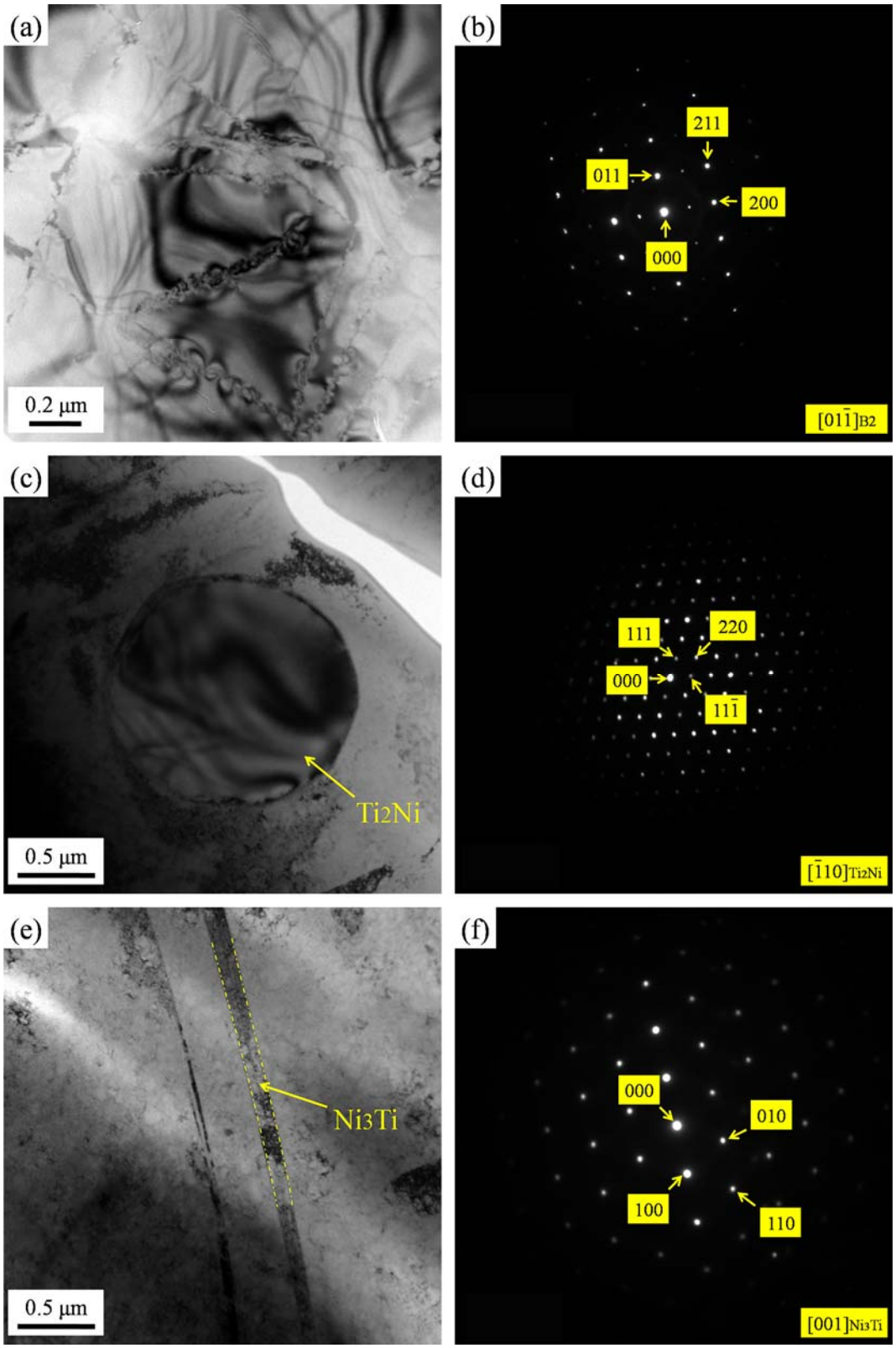

Figure 5. TEM micrographs of $Ni_{44}Ti_{51.8}Fe_{3.2}Ta_1$ SMA: (**a**) Bright field image showing B2 austenite matrix; (**b**) Diffraction pattern of B2 austenite matrix in (**a**); (**c**) Bright field image showing Ti_2Ni precipitate; (**d**) Diffraction pattern of Ti_2Ni precipitate in (**c**); (**e**) Bright field image showing Ni_3Ti precipitate; (**f**) Diffraction pattern of Ni_3Ti precipitate in (**e**).

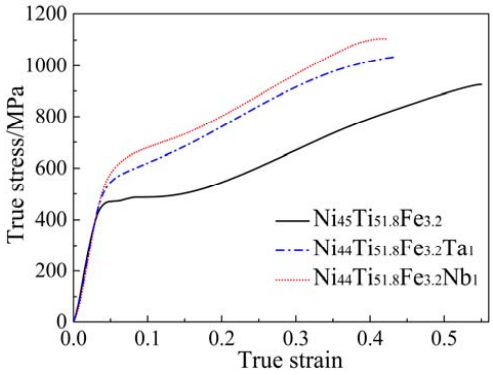

Figure 6. Compressive stress-strain curves of the three NiTi-based SMAs.

3.3. Phase Transformation of NiTi-based SMAs

Figure 7 shows the DSC curves of $Ni_{45}Ti_{51.8}Fe_{3.2}$, $Ni_{44}Ti_{51.8}Fe_{3.2}Nb_1$, and $Ni_{44}Ti_{51.8}Fe_{3.2}Ta_1$ SMAs. All three NiTi-based SMAs exhibit a one-step phase transformation during cooling. The one-step phase transformation deals with the transformation from B2 austenite (A) to B19′ martensite (M). However, all three NiTi-based SMAs exhibit a two-step phase transformation during heating. First, they are converted from B19′ martensite to an R-phase. Subsequently, they are transformed from the R-phase into B2 austenite. It can be noted that the addition of Nb and Ta elements does not change the phase transformation path of NiTiFe SMA, but it does have a certain effect on the transformation temperatures of NiTiFe SMA. As a consequence, all of the transformation temperatures are diminished. In particular, as for $Ni_{44}Ti_{51.8}Fe_{3.2}Nb_1$ SMA, the addition of the Nb element results in the severe diminishment of the martensite and austenite transformation temperatures.

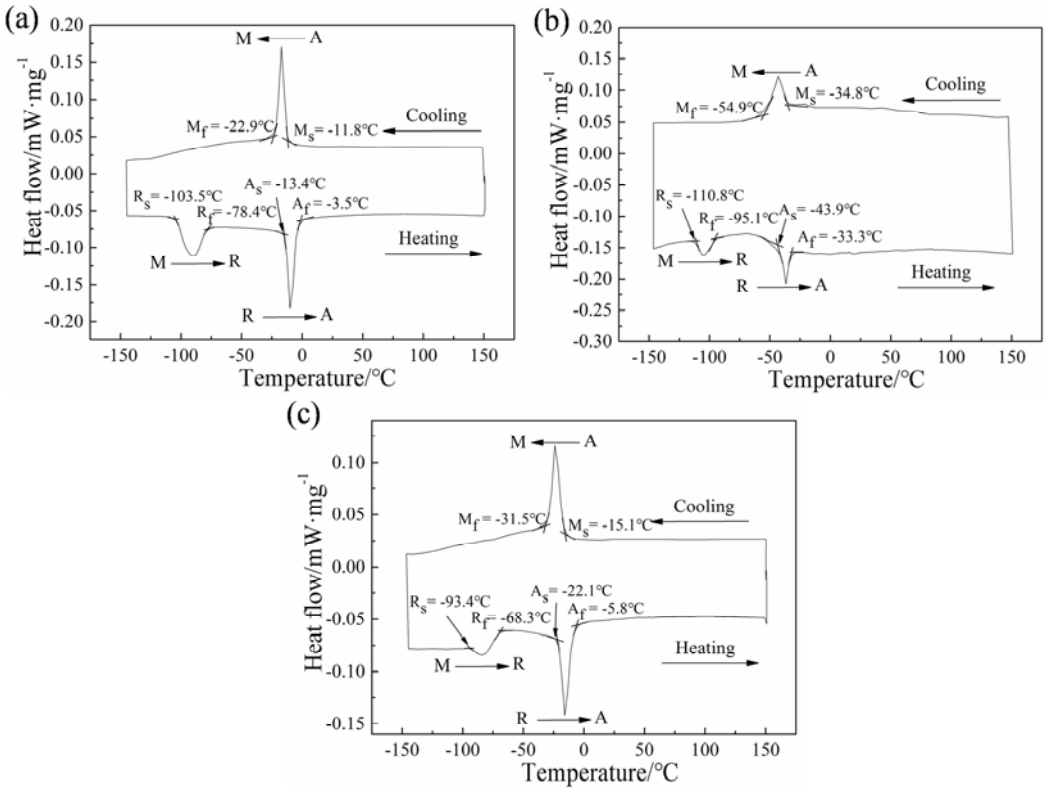

Figure 7. DSC (Differential scanning calorimetry) curves of the three NiTi-based SMAs: (**a**) $Ni_{45}Ti_{51.8}Fe_{3.2}$; (**b**) $Ni_{44}Ti_{51.8}Fe_{3.2}Nb_1$; (**c**) $Ni_{44}Ti_{51.8}Fe_{3.2}Ta_1$.

Compared to $Ni_{45}Ti_{51.8}Fe_{3.2}$ SMA, $Ni_{44}Ti_{51.8}Fe_{3.2}Nb_1$ and $Ni_{44}Ti_{51.8}Fe_{3.2}Ta_1$ SMAs possess a lower phase transformation temperature. In particular, in the case of $Ni_{44}Ti_{51.8}Fe_{3.2}Nb_1$ SMA, the addition of the Nb element influences the phase transformation temperature considerably, and consequently all the phase transformation temperatures are lowered substantially compared with $Ni_{45}Ti_{51.8}Fe_{3.2}$ SMA. In general, for the purpose of lowering the martensite transformation start temperature M_s, the transformation resistance should be enhanced when B2 austenite is transformed into B19′ martensite. Simultaneously, in order to enhance the austenite transformation start temperature A_s, the mechanical driving force should be diminished when B19′ martensite is transformed into B2 austenite.

It can be deduced that the addition of Nb and Ta elements contributes to the increase of the elastic strain energy of B2 austenite. Consequently, the elastic strain energy becomes the resistance, which prevents B2 austenite from being transformed into B19′ martensite, so that the martensite phase transformation temperature is lowered. Conversely, the elastic strain energy kept in the martensite interface becomes the mechanical driving force, which facilitates the transformation from B19′ martensite to B2 austenite, so that the austenite phase transformation temperature is enhanced.

4. Conclusions

Based on ternary $Ni_{45}Ti_{51.8}Fe_{3.2}$ (at %) SMA, two new quaternary $Ni_{44}Ti_{51.8}Fe_{3.2}Nb_1$ and $Ni_{44}Ti_{51.8}Fe_{3.2}Ta_1$ (at %) SMAs were designed and fabricated by adding Nb and Ta elements to replace the Ni element. Furthermore, the microstructure, mechanical property, and phase transformation of NiTiFeNb and NiTiFeTa SMAs were investigated. The following conclusions are drawn:

(1) The microstructures of three NiTi-based SMAs are dominated by equiaxed grains rather than dendrites. $Ni_{45}Ti_{51.8}Fe_{3.2}$ SMA comprises a B2 austenite matrix and a Ti_2Ni precipitate. In the case of $Ni_{44}Ti_{51.8}Fe_{3.2}Nb_1$ SMA, Ti_2Ni and β-Nb precipitates occur in the matrix of B2 austenite. The matrix of $Ni_{44}Ti_{51.8}Fe_{3.2}Ta_1$ SMA belongs to B2 austenite, where Ti_2Ni and Ni_3Ti precipitates can be observed.

(2) The addition of Nb and Ta elements results in the increasing yield strength of NiTi-based SMA, but leads to the decreasing plasticity of NiTi-based SMA. Furthermore, $Ni_{44}Ti_{51.8}Fe_{3.2}Nb_1$ SMA possesses a higher yield strength than $Ni_{44}Ti_{51.8}Fe_{3.2}Ta_1$ SMA, where the Nb element plays a more substantial role in strengthening NiTi-based SMAs compared with the Ta element. Nb and Ta exist in the solid solution of B2 austenite as the solute atoms, since no metallic compounds of Nb and Ta elements are observed in the case of $Ni_{44}Ti_{51.8}Fe_{3.2}Nb_1$. In particular, $Ni_{44}Ti_{51.8}Fe_{3.2}Ta_1$ SMA exhibits a steady strain hardening ability during plastic deformation.

(3) All three NiTi-based SMAs exhibit a one-step phase transformation during cooling, which is involved in the transformation from B2 austenite to B19′ martensite. However, all three NiTi-based SMAs exhibit a two-step phase transformation during heating, where they are converted from B19′ martensite to the R-phase and subsequently they are transformed from the R-phase into the B2 phase. The addition of Nb and Ta elements does not change the phase transformation path of NiTiFe SMA, but it does have a certain effect on the transformation temperatures of NiTiFe SMA. As a consequence, all the transformation temperatures are diminished.

Acknowledgments: The work was financially supported by National Natural Science Foundation of China (Nos. 51475101, 51305091 and 51305092).

Author Contributions: Yulong Liang wrote the manuscript; Shuyong Jiang supervised the manuscript; Yanqiu Zhang performed the OM and TEM analysis; Junbo Yu performed the DSC analysis and compression test.

Conflicts of Interest: The authors declare no conflict of interest.

References

1. Elahinia, M.H.; Hashemi, M.; Tabesh, M.; Bhaduri, S.B. Manufacturing and processing of NiTi implants: A review. *Prog. Mater. Sci.* **2012**, *57*, 911–946. [CrossRef]
2. Sun, L.; Huang, W.M.; Ding, Z.; Zhao, Y.; Wang, C.C.; Purnawali, H.; Tang, C. Stimulus-responsive shape memory materials: A review. *Mater. Des.* **2012**, *33*, 577–640. [CrossRef]
3. Meng, Q.; Yang, H.; Liu, Y.; Nam, T.H. Transformation intervals and elastic strain energies of B2-B19′ martensitic transformation of NiTi. *Intermetallics* **2010**, *18*, 2431–2434. [CrossRef]
4. Otsuka, K.; Ren, X. Physical metallurgy of Ti–Ni-based shape memory alloys. *Prog. Mater. Sci.* **2005**, *50*, 511–678. [CrossRef]
5. Mohd Jani, J.; Leary, M.; Subic, A.; Gibson, M.A. A review of shape memory alloy research, applications and opportunities. *Mater. Des.* **2014**, *56*, 1078–1113. [CrossRef]
6. Etaati, A.; Dehghani, K. A study on hot deformation behavior of Ni–42.5Ti–7.5Cu alloy. *Mater. Chem. Phys.* **2013**, *140*, 208–215. [CrossRef]
7. Nespoli, A.; Villa, E.; Besseghini, S. Characterization of the martensitic transformation in $Ni_{50-x}Ti_{50}Cu_x$ alloys through pure thermal measurements. *J. Alloys Compd.* **2011**, *509*, 644–647. [CrossRef]
8. Goryczka, T.; Ochin, P. Microstructure, texture and shape memory effect in $Ni_{25}Ti_{50}Cu_5$ ribbons and strips. *Mater. Sci. Eng. A* **2006**, *438–440*, 714–718. [CrossRef]
9. He, X.M.; Rong, L.J.; Yan, D.S.; Li, Y.Y. TiNiNb wide hysteresis shape memory alloy with low niobium content. *Mater. Sci. Eng. A* **2004**, *371*, 193–197. [CrossRef]
10. Zhao, X.; Yan, X.; Yang, Y.; Xu, H. Wide hysteresis NiTi (Nb) shape memory alloys with low Nb content (4.5 at %). *Mater. Sci. Eng. A* **2006**, *438*, 575–578. [CrossRef]
11. Shu, X.Y.; Lu, S.Q.; Li, G.F.; Liu, J.W.; Peng, P. Nb solution influencing on phase transformation temperature of Ni47Ti44Nb9 alloy. *J. Alloys Compd.* **2014**, *609*, 156–161. [CrossRef]
12. Xue, S.; Wang, W.; Wu, D.; Zhai, Q.; Zheng, H. On the explanation for the time-dependence of B2 to R martensitic transformation in $Ti_{50}Ni_{47}Fe_3$ shape memory alloy. *Mater. Lett.* **2012**, *72*, 119–121. [CrossRef]
13. Basu, R.; Eskandari, M.; Upadhayay, L.; Mohtadi-Bonab, M.A.; Szpunar, J.A. A systematic investigation on the role of microstructure on phase transformation behavior in Ni–Ti–Fe shape memory alloys. *J. Alloys Compd.* **2015**, *645*, 213–222. [CrossRef]
14. Matsuda, M.; Yamashita, R.; Tsurekawa, S.; Takashima, K.; Mitsuhara, M.; Nishida, M. Antiphase boundary-like structure of B19′ martensite via R-phase transformation in Ti–Ni–Fe alloy. *J. Alloys Compd.* **2014**, *586*, 87–93. [CrossRef]
15. Kovarik, L.; Yang, F.; Garg, A.; Diercks, D.; Kaufman, M.; Noebe, R.D.; Mills, M.J. Structural analysis of a new precipitate phase in high-temperature TiNiPt shape memory alloys. *Acta Mater.* **2010**, *58*, 4660–4673. [CrossRef]
16. Atli, K.C.; Karaman, I.; Noebe, R.D.; Maier, H.J. Comparative analysis of the effects of severe plastic deformation and thermomechanical training on the functional stability of $Ti_{50.5}Ni_{24.5}Pd_{25}$ high-temperature shape memory alloy. *Scr. Mater.* **2011**, *64*, 315–318. [CrossRef]
17. Santamarta, R.; Arróyave, R.; Pons, J.; Evirgen, A.; Karaman, I.; Karaca, H.E.; Noebe, R.D. TEM study of structural and microstructural characteristics of a precipitate phase in Ni-rich Ni–Ti–Hf and Ni–Ti–Zr shape memory alloys. *Acta Mater.* **2013**, *61*, 6191–6206. [CrossRef]
18. Kockar, B.; Karaman, I.; Kim, J.I.; Chumlyakov, Y. A method to enhance cyclic reversibility of NiTiHf high temperature shape memory alloys. *Scr. Mater.* **2006**, *54*, 2203–2208. [CrossRef]
19. Rehman, S.U.; Khan, M.; Nusair Khan, A.; Ali, L.; Zaman, S.; Waseem, M.; Ali, L.; Jaffery, S.H.I. Transformation behavior and shape memory properties of $Ti_{50}Ni_{15}Pd_{25}Cu_{10}$ high temperature shape memory alloy at various aging temperatures. *Mater. Sci. Eng. A* **2014**, *619*, 171–179. [CrossRef]
20. Karaca, H.E.; Acar, E.; Ded, G.S.; Saghaian, S.M.; Basaran, B.; Tobe, H.; Kok, M.; Maier, H.J.; Noebe, R.D.; Chumlyakov, Y.I. Microstructure and transformation related behaviors of a $Ni_{45.3}Ti_{29.7}Hf_{20}Cu_5$ high temperature shape memory alloy. *Mater. Sci. Eng. A* **2015**, *627*, 82–94. [CrossRef]
21. Hong, S.H.; Kim, J.T.; Park, H.J.; Kim, Y.S.; Suh, J.Y.; Na, Y.S.; Lim, K.R.; Shim, C.H.; Park, J.M.; Kim, K.B. Influence of Zr content on phase formation, transition and mechanical behavior of Ni–Ti–Hf–Zr high temperature shape memory alloys. *J. Alloys Compd.* **2017**, *692*, 77–85. [CrossRef]

22. Prasad, R.V.S.; Park, C.H.; Kim, S.W.; Hong, J.K.; Yeom, J.T. Microstructure and phase transformation behavior of a new high temperature NiTiHf-Ta shape memory alloy with excellent formability. *J. Alloys Compd.* **2017**, *697*, 55–61. [CrossRef]
23. Acar, E.; Karaca, H.E.; Tobe, H.; Noebe, R.D.; Chumlyakov, Y.I. Characterization of the shape memory properties of a $Ni_{45.3}Ti_{39.7}Hf_{10}Pd_5$ alloy. *J. Alloys Compd.* **2013**, *578*, 297–302. [CrossRef]
24. Karaca, H.E.; Acar, E.; Ded, G.S.; Basaran, B.; Tobe, H.; Noebe, R.D.; Bigelow, G.; Chumlyakov, Y.I. Shape memory behavior of high strength NiTiHfPd polycrystalline alloys. *Acta Mater.* **2013**, *61*, 5036–5049. [CrossRef]
25. Meng, X.L.; Li, H.; Cai, W.; Hao, S.J.; Cui, L.S. Thermal cycling stability mechanism of $Ti_{50.5}Ni_{33.5}Cu_{11.5}Pd_{4.5}$ shape memory alloy with near-zero hysteresis. *Scr. Mater.* **2015**, *103*, 30–33. [CrossRef]
26. Schmidt, M.; Ullrich, J.; Wieczorek, A.; Frenzel, J.; Schütze, A.; Eggeler, G.; Seelecke, S. Thermal stabilization of NiTiCuV shape memory alloys: Observations during elastocaloric training. *Shape Mem. Superelast.* **2015**, *1*, 132–141. [CrossRef]